

ULRR

The formation of three-grain junctions during solidification. Part II: theory

Item Type	Article
Authors	Fowler, Andrew;Holness, Marian B.
Citation	Contributions to Mineralogy and Petrology (2022) 177 (58)
Publisher	Springer
Download date	2026-04-12 12:11:22
Item License	https://creativecommons.org/licenses/by-nc-sa/4.0/
Link to Item	https://doi.org/10.34961/researchrepository-ul.25274128



The formation of three-grain junctions during solidification. Part II: theory

A. C. Fowler^{1,2} · Marian B. Holness³

Received: 3 August 2021 / Accepted: 15 April 2022 / Published online: 7 June 2022
© The Author(s) 2022

Abstract

We provide a simple geometric theory of crystal growth which predicts the shape and final dihedral angle of three-grain junctions of an augite crystal with two plagioclase grains. The predicted dihedral angle Δ depends on the initial impingement angle ψ formed by the plagioclase grains, and also on the relative growth rates of the augite and the plagioclase, and shows reasonable agreement with data obtained from natural samples. We show that the two augite-plagioclase grain boundaries will normally curve towards each other, which is consistent with the first two types of junction described in the companion paper. However, the third type, the eagle's beak, is formed by the meeting of grain boundaries which curve in the same direction. Although it is possible to account for this type of junction by invoking the localised dissolution of one of the plagioclase grains, this is unlikely to occur. A more plausible explanation involves the late impingement of the two plagioclase grains, consistent with the observation that eagles' beaks are common in gabbros and strongly orthocumulate troctolites, in which the plagioclase framework has not been established by the time augite is growing in substantial quantities. An observed flattening of the curve of Δ values at high values of ψ can be explained by taking into account the importance of interfacial energy in late-stage crystallisation.

Keywords Magma crystallisation · Dihedral angle · Melt-back

Introduction

In the companion paper, we described the shapes of three-grain junctions of augite, A, with plagioclase, P, in various dolerites and gabbros, as viewed in 2D thin sections. We identified three distinct geometric types of junction, as indicated in Fig. 1. Type 1 junctions involve the meeting of two planar AP interfaces, and type 2 junctions are formed by the meeting of two AP interfaces which curve towards each other. While these first two types are symmetric, the third type is not, and involves the meeting of two AP interfaces which curve in the same direction: we term this third type the eagle's beak and it is common in gabbroic cumulates.

The first two types of junction are seen in dolerites, with the extent of curvature of the two AP interfaces a function of cooling rate. The dihedral angle is formed by the growth of augite into the pore corner formed by the impingement of the two plagioclase grains, with the final geometry controlled by the relative rate of growth of the two phases (Holness 2015): we showed in the companion paper that the final angle usually exceeds the angle at which the two plagioclase grains originally impinged. Furthermore, in slowly cooled troctolitic cumulates, the extent of asymmetry of the junction is dependent on the amount of interstitial liquid. Type 2 junctions are found in adcumulates, but the asymmetry of the junctions increases towards type 3 (eagle's beak) geometries typical of gabbroic cumulates with an increasing amount of interstitial liquid. The geometry of APP junctions is clearly a function not only of cooling rate but also of the extent to which augite is a framework-forming phase in these mafic cumulates. Sketched examples of the three-grain junction morphologies we seek to explain, taken from a gabbro from the Skaergaard Intrusion, East Greenland, are shown in Fig. 2 and in this paper we develop a simple

Communicated by Timothy L. Grove.

✉ A. C. Fowler
fowler@maths.ox.ac.uk

¹ MACSI, University of Limerick, Limerick, Ireland

² OCIAM, University of Oxford, Oxford, UK

³ Department of Earth Science, University of Cambridge, Cambridge, UK

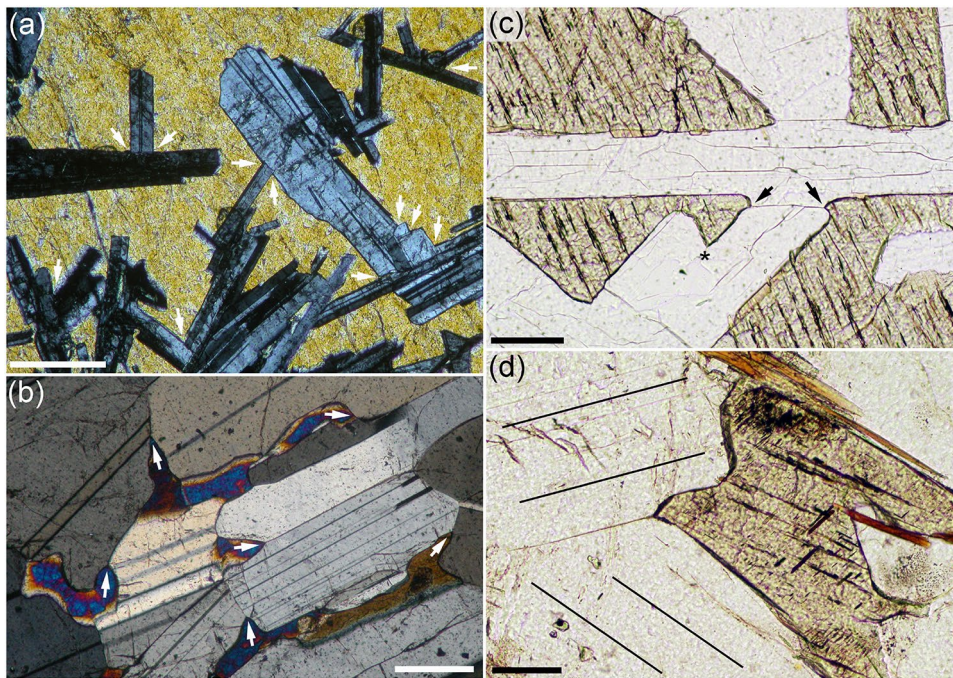


Fig. 1 Photomicrographs illustrating the three different types of APP junction. **a** Dolerite from the Camas Malag dyke, Skye photographed under crossed polars. Poikilitic clinopyroxene encloses numerous plagioclase chadacrysts. The APP three-grain junctions are all of Type 1, and are formed by the impingement of planar augite-plagioclase grain boundaries, with no curvature or deflection as the junction is approached (examples are arrowed). The scale bar is 0.2 mm long. **b** A troctolite from the Rum Eastern Layered Intrusion, photographed under plane polarised light. Augite is interstitial. APP junctions are formed of non-planar augite-plagioclase grain boundaries, which curve towards each other as the APP three-grain junction is approached, forming a symmetrical geometry of Type 2. Examples are marked by arrows. The scale bar is 0.2 mm long. **c** Gabbro from

the Layered Series of the Skaergaard Intrusion, in which both augite and plagioclase are primocrysts, photographed in plane polarised light. The two arrowed APP three-grain junctions are formed by the meeting of two augite-plagioclase grain boundaries that curve in the same sense in the immediate vicinity of the junction: these junctions are Type 2, the eagle's beak. The APP junction marked by an asterisk is of Type 2. The scale bar is 0.5 mm long. **d** Gabbro from the Layered Series of the Skaergaard Intrusion, photographed in plane polarised light. The APP three-grain junction in the centre of the image is of Type 3, an eagle's beak. The orientation of the (010) twin planes in the two plagioclase grains is denoted by black lines. The scale bar is 0.1 mm long

geometric growth model of crystallisation to account for these observations.

Three-grain junction formation

The setting for our study is the crystal mushy layer that forms on the margins of magma chambers. Such mushes form either by crystal settling or by in situ nucleation and growth. We do not consider fluid convection within the mush, and assume that the crystals themselves are stationary and that the mush is not being deformed either by compaction or by shearing. In our description, the final shape of the grain interfaces is thus solely determined by the kinetics of crystal growth.

We first consider the case where an augite crystal grows towards two plagioclase crystals which have already fused to form a plagioclase-plagioclase grain boundary (Fig. 3): we will show that a simple model involving simultaneous

growth of augite and plagioclase can account for the second type of three-grain junctions described above. (The first type is simply a particular case of the second type, in which the plagioclase interfaces are stationary.)

Plagioclase crystals are tabular, and appear rectangular in thin section. The relative rates of growth of the edges and faces of the tablets are a function of cooling rate (Holness 2014). Augite crystals are generally equant (e. g., as seen in quenched partially crystallised material such as the crust of the Kilauea Iki lava lake: Fig. 5 of Holness et al. 2012) and, although the equant grains are indeed partially faceted, the significant difference between the overall shapes of the plagioclase and associated augite justifies the simplification of assuming augite grows as non-faceted spherical crystals, with growth rate independent of crystallographic orientation.

To solve the geometric growth problem, we consider a symmetric geometry shown in Fig. 4. We suppose that two plagioclase crystals with an internal (impingement) angle

Fig. 2 Sketches of four high dihedral angle junctions formed by two plagioclase grains (P) and one augite grain (A), from a gabbro from the Skaergaard Intrusion, East Greenland, showing how curvature of the grain boundaries in the immediate vicinity of the three-grain junction affects the final dihedral angle. Each sketch is approximately 0.1 mm across. In cases (a–c), the impingement angle is large, and it can be seen that a late reduction in Δ below ψ is facilitated by inward bending (in red) of one of the A–P grain boundaries towards the plagioclase grain. **d** is rather different. It appears to be en route to form an eagle’s beak, similarly to (a). But then apparently, the augite stops growing (blue line). We might associate this apparent cessation with the high dihedral angle flattening mechanism in Sect. 4

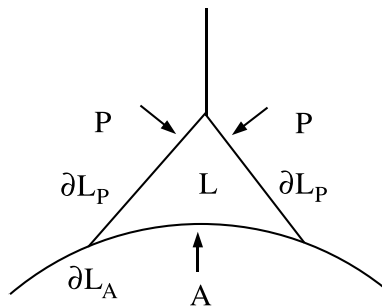
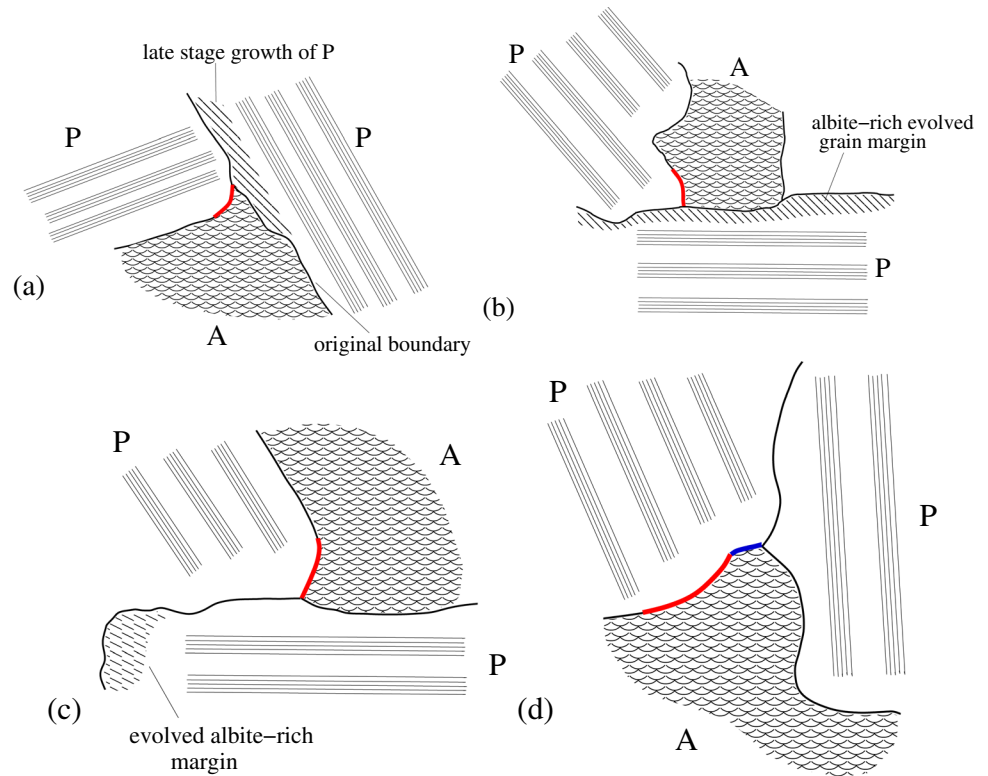


Fig. 3 Growth geometry of two plagioclase crystals, with an adjoining augite crystal. L denotes the interstitial liquid

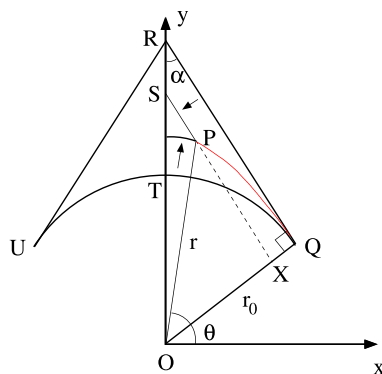


Fig. 4 Geometry of the solution

$\psi = 2\alpha$ crystallise at speed v_p . The interfaces are presumed flat (and without loss of generality, two-dimensional). Earlier, an augite crystal is nucleated and grows as a spherical crystal, until at some time, which we take as $t = 0$, it touches the plagioclase crystals. We suppose the augite crystal is of initial radius r_0 . The two geometric parameters of the problem are thus r_0 and α .

If v_A and v_p are variable in time, it is convenient to normalise time by defining a new variable τ via

$$\tau = \int_0^t v_A(s) ds, \tag{2.1}$$

note that the units of τ are those of distance. With respect to this new variable, the augite-melt interfaces move at speed one, while the speed of the plagioclase-melt interface is

$$\gamma = \frac{v_p}{v_A}; \tag{2.2}$$

augite generally grows more rapidly, in which case $\gamma < 1$.

In Fig. 4, the plagioclase interfaces are initially at UR and RQ, and the equation of RQ is

$$x \cos \alpha + y \sin \alpha = r_0. \tag{2.3}$$

The initial augite interface UTQ is at $r = r_0$, where r is the polar radius. At time τ later, the right hand plagioclase interface has moved to PS, on which

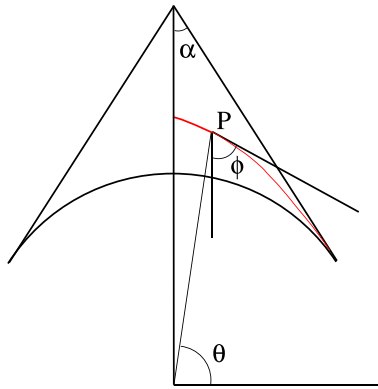


Fig. 5 The relationship of the inclination angle ϕ to the polar angle θ

$$x \cos \alpha + y \sin \alpha = r_0 - \int_0^t v_P(s) ds = r_0 - \int_0^\tau \gamma(\xi) d\xi, \tag{2.4}$$

while the augite interface moves out uniformly, and is given by

$$r = r_0 + \tau. \tag{2.5}$$

The point where the two interfaces join is P, and it thus traces out a path QP which satisfies both (2.4) and (2.5). Eliminating τ , this gives the equation in polar coordinates

$$r = R(\theta), \quad R \cos(\theta - \alpha) = r_0 - \int_0^{R-r_0} \gamma(\xi) d\xi, \tag{2.6}$$

if, as an example, we suppose that γ is constant, this gives

$$\frac{(1 + \gamma)r_0}{\gamma R} = 1 + \frac{1}{\gamma} \cos(\theta - \alpha), \tag{2.7}$$

which is the equation of a conic section of eccentricity $1/\gamma$. To obtain the equation of the left hand interface, we simply replace θ by $\pi - \theta$, thus

$$\frac{(1 + \gamma)r_0}{\gamma R} = 1 - \frac{1}{\gamma} \cos(\theta + \alpha). \tag{2.8}$$

It is clear that the angle α need not be the same on each side, which corresponds to the case of asymmetric growth.

Of interest is the final dihedral angle, which we will denote as Δ , so that $\Delta = 2\phi|_{\theta=\pi/2}$ (see Fig. 5). This is given via

$$\tan \phi = -\frac{dx}{dy}, \tag{2.9}$$

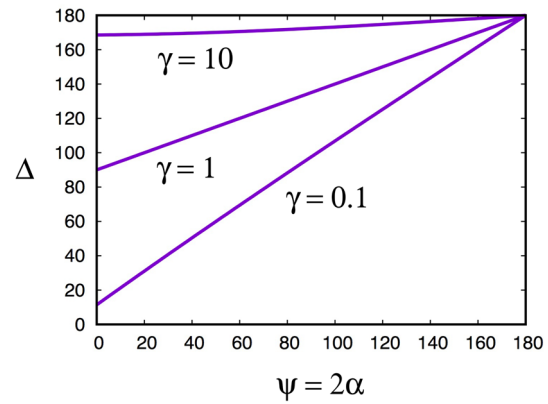


Fig. 6 The final dihedral angle $\Delta = 2\phi$ as a function of the initial impingement angle of separation $\psi = 2\alpha$, for various values of γ , assuming symmetric prograde crystallisation. The units are degrees

and the expression is then to be evaluated at $x = 0$. Carrying out the calculation (see the electronic supplementary material), we have

$$\tan \phi = \frac{\gamma \sin \theta + \sin \alpha}{\gamma \cos \theta + \cos \alpha}. \tag{2.10}$$

To calculate the final dihedral angle, we put $\theta = \frac{1}{2}\pi$, to find

$$\Delta = 2 \tan^{-1} \left[\frac{\gamma + \sin \alpha}{\cos \alpha} \right]. \tag{2.11}$$

It is straightforward to allow γ to vary in time, using (2.6); in that case the value of γ in (2.11) is its final value. Δ is thus an increasing (and more or less linear) function of the initial plagioclase angle of separation $\psi = 2\alpha$, and is shown in Fig. 6. This figure can be compared with the data shown in Fig. 5 of part 1. We see that there is good agreement if $\gamma < 1$, that is, $v_P < v_A$ as we expect, provided $\psi \lesssim \Theta_{\text{cpp}}^* = 109^\circ$, where this last quantity is the equilibrium dihedral angle (Holness et al. 2012). Above this value, there are few data points, but those there are appear to show a levelling off, with $\Delta \approx \Theta_{\text{cpp}}^*$. We return to this issue later.

The distance $X = r \cos(\theta - \alpha)$ of the point P along the line OQ (i. e., the length of OX in Fig. 4) satisfies

$$\frac{dX}{dr} = -\gamma < 0, \tag{2.12}$$

and thus as shown in Fig. 4 the interface curves to the left. This is discussed further below.

Eagles' beaks

Eagles' beaks are the type 3 junction, for which the two AP grain boundaries have their curvature *in the same direction* (Fig. 1c, d). If we denote the half-angle on the right in Figure 5 as α_+ , and the corresponding half-angle on the left as α_- (thus allowing for asymmetric growth), then the curve on the left is given by (2.8), thus

$$\frac{(1 + \gamma_-)r_-}{\gamma_-R} = 1 - \frac{1}{\gamma_-} \cos(\theta + \alpha_-), \tag{3.1}$$

while the curve on the right is given by (2.7), thus

$$\frac{(1 + \gamma_+)r_+}{\gamma_+R} = 1 + \frac{1}{\gamma_+} \cos(\theta - \alpha_+). \tag{3.2}$$

Both (3.1) and (3.2) represent conic sections, and we pause to recall some basic geometric facts. The curve (in polar coordinates, where $\theta = 0$ is horizontal)

$$\frac{ed}{r} = 1 - e \cos \theta. \tag{3.3}$$

is a conic of eccentricity e , and for $e > 1$ (as here) it represents one branch of a (C-shaped) hyperbola. It is the locus of points P for which the ratio PF/PD = e is constant, where F is the focus, and taken to be the origin, and PD is the distance from P to the vertical line D (the directrix) which is a distance d to the left of F. The hyperbola curves to the right, and the two asymptotes are the rays $\theta = \pm \cos^{-1} \left(\frac{1}{e} \right)$. Thus if $\gamma_- < 1$, the curve given by (3.1) represents such a hyperbola, rotated clockwise by an angle α_- .

Similarly, the curve (3.2) represents a hyperbola which bends to the left, and thus if $0 < \gamma_-, \gamma_+ < 1$, the right and left interfaces curve towards each other, as in Fig. 1b. In the situation indicated in Fig. 4, where the plagioclase grains have already impinged, the only way an eagle's beak can form is if one of the growth rates is negative, i. e., melt-back occurs. Specifically, if we suppose $\gamma_+ < 0$, the right hand hyperbola also becomes C-shaped, and an eagle's beak can form. However, it is not clear how (or why) such disparate behaviour of neighbouring grains could occur.

Non-impinged plagioclase grains

Now consider the situation where a growing augite crystal impinges on a plagioclase crystal as shown in Fig. 7, where the upper half-length of the tabular face is l , and the augite crystal is of initial radius r_0 . We suppose the tabular (long) face grows at a rate γ_\perp , while the (short) end face grows at a rate $\gamma_\parallel > \gamma_\perp$, but both growth rates are less than one (i. e., less than that of augite). Initially the augite-plagioclase grain boundary (which we will henceforth refer to as the A-P grain

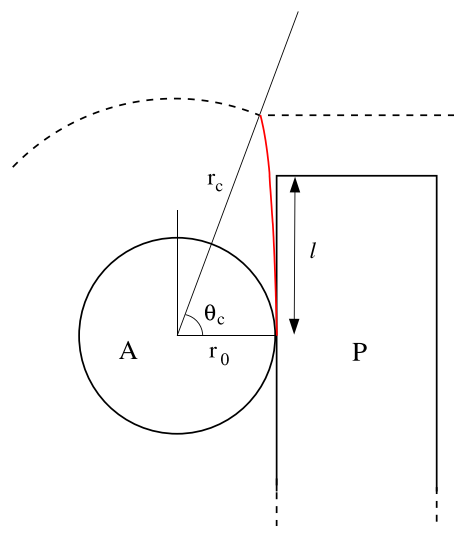


Fig. 7 Initial impingement of augite (A) and plagioclase (P) is shown by the solid circular and rectangular crystals. The (red) interface grows along the tabular face until it reaches the short end face (dashed lines)

boundary) curves to the left and is given by (3.2), which we write in the form

$$\gamma_\perp + \cos \theta = \frac{r_0(1 + \gamma_\perp)}{r}. \tag{3.4}$$

At the same time the top (short) face is given by $y = l + \gamma_\parallel \tau$, and hence (since $r = r_0 + \tau$)

$$\sin \theta - \gamma_\parallel = \frac{l - \gamma_\parallel r_0}{r}, \tag{3.5}$$

and thus the augite crystal reaches the corner of the plagioclase crystal when $r = r_c$ and $\theta = \theta_c$, and both (3.4) and (3.5) are satisfied. This gives an equation for θ_c which is

$$\sin \theta_c - \gamma_\parallel = \left(\frac{l}{r_0} - \gamma_\parallel \right) \left(\frac{\gamma_\perp + \cos \theta_c}{1 + \gamma_\perp} \right), \tag{3.6}$$

which always has a unique solution for $\theta_c \in \left(0, \frac{\pi}{2} \right)$ [compare the graphs of the two sides of (3.6)]. The geometry of the situation is shown in Fig. 7. Note that in terms of r_c and θ_c , the grain boundary formula (3.4) can be written in the form

$$\cos \theta + \gamma_\perp = \frac{r_c(\cos \theta_c + \gamma_\perp)}{r}. \tag{3.7}$$

Growth at a corner

What happens when the grain boundary reaches the corner of the plagioclase? One possibility is that the grain boundary

continues round the corner and marches along the short end of the plagioclase grain. It is simple to show in this case that the grain boundary is given by

$$\sin \theta - \gamma_{\parallel} = \frac{r_c (\sin \theta_c - \gamma_{\parallel})}{r} \tag{3.8}$$

For both cases $\theta_c \geq \sin^{-1} \gamma_{\parallel}$ (corresponding to $l \geq \gamma_{\parallel} r_0$ —see (3.6)), this gives a hyperbola which curves upwards. However, there is a slope discontinuity at the corner. We can use the formulae (3.7) and (3.8) to calculate the slopes using the same method as in the electronic supplementary material (see Eq. (ESM1.3) there). The result of this is that on the pre-corner sub-vertical boundary, the slope is

$$\frac{dy}{dx} = -\frac{(1 + \gamma_{\perp} \cos \theta)}{\gamma_{\perp} \sin \theta}, \tag{3.9}$$

whereas after passage through the corner, on the sub-horizontal boundary,

$$\frac{dy}{dx} = \frac{\gamma_{\parallel} \cos \theta}{1 - \gamma_{\parallel} \sin \theta}, \tag{3.10}$$

and these two slopes are clearly discontinuous (for a start they have opposite signs).

We do not observe such slope discontinuities in thin sections, and we do not think they occur. What happens then? Our answer to this takes us technically to places beyond the scope of this paper, and even of the Electronic Supplementary Material, and we hope to develop it further in a theoretical paper. But we can provide an outline of our reasoning.

Facetting

We need to consider in more detail the growth rate of the plagioclase crystals. These are faceted, and this is a consequence of the idea that the surface growth rate is a function of its orientation χ , where $\chi = \pi/2$ corresponds to the (long) vertical face, and $\chi = 0$ to the (short) horizontal face, and $\gamma(0) = \gamma_{\parallel}$, $\gamma(\frac{\pi}{2}) = \gamma_{\perp}$. Facetting occurs because an inclined surface with $0 < \chi < \frac{1}{2}\pi$ is rough and has higher surface energy and thus higher growth rate than the smooth vertical and horizontal surfaces (Flemings 1974). In a simple growth rate model where the normal velocity is thus $v_n = \gamma(\chi)$, slope discontinuities and hence facets are predicted to occur.

The growth rate of crystal interfaces is controlled by kinetic undercooling,¹ but the thermodynamic equilibrium

¹ As opposed to heat or compositional transfer (Dowty 1980); this is because of the observed difference in growth rates of the different plagioclase faces.

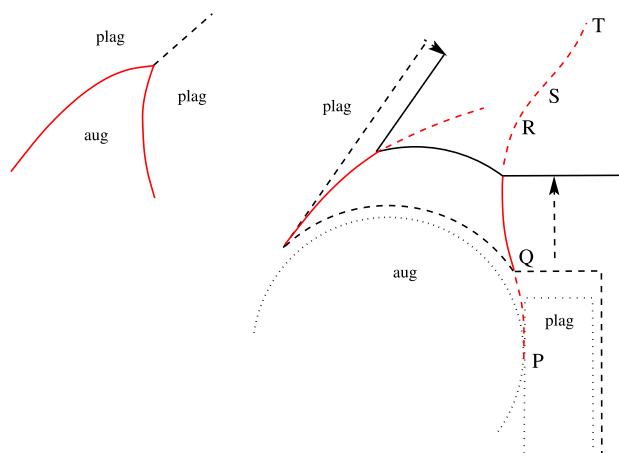


Fig. 8 A schematic representation of the formed beak and its forming process. Impingement occurs at P when the dotted grains touch. Thereafter, the A–P grain boundary PQ forms a type 2 interface, but when the augite reaches the corner of the plagioclase grain at Q, it gets locked to the corner while the interface angle χ decreases towards 0. Eventually (at R), the angle θ measured from the centre of the augite reaches a maximum, but note that the curvature must already change before that (QR). If χ reaches 0 (at S), then the augite can progress along the short end of the plagioclase, and the curvature will reverse (ST), but close-off may have already occurred by then due to the advancing left hand plagioclase grain

temperature depends on the surface curvature through the Gibbs-Thomson effect (Davis 2001), and the consequent (small) effect of this on the growth rate provides a diffusive effect which smoothes out the apparent discontinuity in slope at a faceted corner at a small length scale.

What we propose is that when the augite reaches the corner of the plagioclase, it does not immediately proceed round the corner, but instead experiences a ‘waiting time’ (Lacey et al. 1982; Kath and Cohen 1982) while the interfacial growth angle χ gradually changes from $\frac{\pi}{2}$ to 0. As explained in the electronic supplementary material, this reduction in χ causes a change in the behaviour of the polar angle θ , which will eventually start to decrease as the augite makes its way along the short face of the plagioclase. A full justification of this description requires an analysis of the combined growth of the crystals which is similar to Jackson and Hunt’s (1966) theory of lamellar eutectic growth, but which is deferred to a future theoretical paper. A glimpse of the technical detail can be found in the electronic supplementary material.

The result of this description is illustrated schematically in Fig. 8. Following impingement at P, the grain boundary curves inwards until it reaches the corner at Q. Thereafter, the slope angle χ changes gradually from $\frac{\pi}{2}$ to 0 as the interface moves from Q to S, and after that it will move along the short end, with a resumption of curving to the left along ST. In the illustration, this last part would not occur, since pore close-off by the grain on the left will form the eagle’s

beak at S. This process is our proposed mechanism for the formation of eagles' beaks.

Dihedral angle flattening

We now turn our attention to the data shown in Fig. 5 of part 1, which shows an apparent flattening of the final dihedral angle Δ at high values of the impingement angle ψ . The simple model of three-grain junction formation predicts that the final dihedral angle will always be equal to, or greater than, the initial angle created by the impingement of the two plagioclase grains, whereas the data presented in Fig. 5 of part 1 (and illustrated in Fig. 2a–c) suggests that this is not the case, and that for initially very large impingement angles the final dihedral angle is generally smaller.

Figure 6 clearly shows that for $\gamma < 1$, i. e., $v_p < v_A$, the predicted dihedral angle Δ is greater than the impingement angle ψ , and for $\psi \lesssim 100^\circ$, and allowing for a range of γ , the agreement with the data in Fig. 5 of part 1 is encouraging. But there is one feature of this data which is of concern, and this is the fact that the observed values of dihedral angle in dolerites and gabbros, Δ , appear to be generally lower than about 120° , and particularly, when $\psi > \Theta_{\text{cpp}}^*$, the equilibrium dihedral angle, $\Delta \lesssim \Theta_{\text{cpp}}^*$. This is inconsistent with our purely geometric theory of crystal growth, and further suggests that the equilibrium dihedral angle somehow exerts an influence, which seems to contradict our thesis. However, we saw in the preceding section that surface energy can become critically important in the late stages of crystallisation. In this section we enunciate a theory to address this issue.

The thermodynamic theory of homogeneous nucleation demonstrates that interfacial energy provides a barrier to the nucleation of crystals, which can be minimised by heterogeneous nucleation (Dowty 1980; Kelton and Greer 2010). In order for a crystal to nucleate, the free energy of the crystal plus liquid must be less than when the medium is entirely liquid. The nucleation of a (spherical) crystal of radius R causes a reduction of the free energy proportional to the volume of the crystal, i. e., $\propto R^3$, but at the expense of creating new interfacial energy proportional to the interfacial area, i. e., $\propto R^2$. Thus, for small R the interfacial energy provides a barrier to nucleation, which can be overcome by supersaturation of the liquid. Evidently a similar energy barrier may need to be overcome in the last stages of solidification, since one is replacing solid–liquid interfaces with solid–solid interfaces. Whether an energy barrier actually exists will depend on the relative magnitudes of the various interfacial energies involved.

It has not often been considered, if at all, that this consideration must come into play when crystallisation proceeds to completion: the free energy of the solid plus liquid must decrease. Generally, the free energy is controlled volumetrically, and in particular, the evolving dihedral angles are controlled by

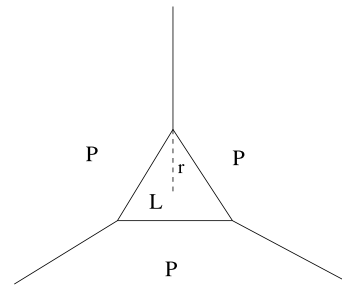


Fig. 9 Planar growth of three P crystals with interstitial liquid L

macroscopic growth rates dependent on interfacial supercooling, for example; but as the liquid fraction shrinks to zero, interfacial energy considerations must become dominant. We now consider an idealised example of this situation.

Planar growth

Let us consider the planar growth of a pure material P in the geometry shown in Fig. 9. Three grains approach each other prismatically as shown, and we will suppose the prismatic cross section is an equilateral triangle, whose circumcircle has radius r . If the chemical potentials of liquid and solid are μ_L and μ_S , and $\Delta\mu = \mu_L - \mu_S$, then some elementary geometry (see the Electronic Supplementary Material) shows that the free energy per unit length of the prism relative to the solid state is

$$\Delta G = \frac{3\sqrt{3}r^2\Delta\mu}{4V_M} + 3(\sigma_{\text{PL}}\sqrt{3} - \sigma_{\text{PP}})r, \quad (4.1)$$

where σ_{PL} and σ_{PP} are the energies of the solid–liquid and solid–solid interfaces, respectively, and V_M is the molar volume of the liquid.

As crystallisation proceeds, ΔG must decrease, and we can immediately see that there is a problem if $\sigma_{\text{PP}} > \sigma_{\text{PL}}\sqrt{3}$, for then ΔG reaches a minimum at positive r . Note that the equilibrium dihedral angle Θ satisfies $\sigma_{\text{PP}} = 2\sigma_{\text{PL}}\cos\frac{1}{2}\Theta$ (see the Electronic Supplementary Material), and thus the problem occurs if $\Theta < 60^\circ$.

We can generalise this result for arbitrarily shaped triangles. At any grain–grain–liquid corner with an impingement angle of θ (i. e., θ is the angle subtended in the liquid), local growth of the grain boundary requires that the interfacial energy decrease,² and this requires $\theta < \Theta$. Since the sum of the angles of a triangle is 180° , we again see that planar

² The point here is that, even if the system is not in chemical equilibrium (i. e., crystal growth is occurring), the assumption of *local* equilibrium presumes that growth can only occur at a grain–grain–liquid junction if the result of grain growth is a local diminution of surface energy.

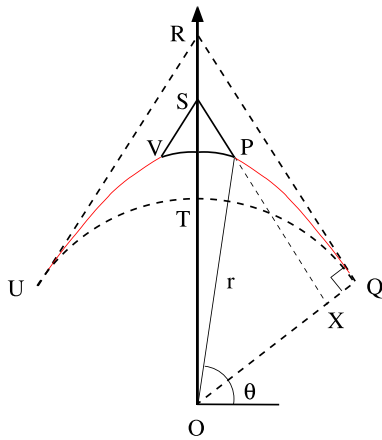


Fig. 10 Calculation of surface energy

interfacial growth must cease if $\Theta < 60^\circ$ (which is commonly the case in basaltic melts).

What then? In order for crystallisation to proceed past the resultant minimum of ΔG , the geometric configuration of the liquid-filled pore must change in some way. One way in which this can be done is if the symmetry is broken and the triangle becomes isosceles; a further possibility is that the interfaces become curved. We do not pursue the consequences for a single phase, but return to the situation under consideration, that of augite-plagioclase-plagioclase (APP) growth.

APP growth

We now revert to the geometry shown in Fig. 4, but now partly redrawn in Fig. 10. The initial configuration of the interfaces is the dotted line UTQR, and at time t later, this has become PSV. The interfacial energy (per unit length) at time t (or ‘time’ τ) relative to its initial value is

$$E = \sigma_{PP}RS + 2\sigma_{AP}PQ + \sigma_{AL}PV + 2\sigma_{PL}PS. \tag{4.2}$$

After a geometric calculation (see the Electronic Supplementary Material), this gives

$$E = \frac{\sigma_{PP} \int_0^\tau \gamma(s) ds}{\sin \alpha} + 2\sigma_{AP} \int_\alpha^\theta [R'(\theta')^2 + R(\theta')^2]^{1/2} d\theta' + 2\sigma_{AL} \left(\frac{\pi}{2} - \theta\right) R(\theta) + \frac{2\sigma_{PL} R(\theta) \cos \theta}{\sin \alpha}, \tag{4.3}$$

where the polar coordinates of P are $r = R(\theta)$ and θ , and these are related to each other and to τ by (2.5) and (2.6) (allowing γ to be variable in time, and thus a function of τ):

$$R = r_0 + \tau, \quad R \cos(\theta - \alpha) = r_0 - \int_0^{R-r_0} \gamma(\tau) d\tau. \tag{4.4}$$

Next we calculate the volume of melt (per unit length): this is

$$V = R^2 \left[\frac{\cos \theta \cos(\theta - \alpha)}{\sin \alpha} - \left(\frac{\pi}{2} - \theta\right) \right], \tag{4.5}$$

then the free energy per unit length of the system, relative to a reference value, is

$$\Delta G = \frac{V\Delta\mu}{V_M} + E. \tag{4.6}$$

Therefore the rate of change of ΔG can be calculated, and this is

$$\begin{aligned} \frac{\partial \Delta G}{\partial \tau} = & -\frac{R\Delta\mu}{V_M} \left[\frac{2\gamma \cos \theta}{\sin \alpha} + \pi - 2\theta \right] + \frac{\sigma_{PP}\gamma}{\sin \alpha} + 2\sigma_{AP}(1 + \Gamma^2)^{1/2} \\ & + 2\sigma_{AL} \left(\frac{\pi}{2} - \theta - \Gamma\right) + \frac{2\sigma_{PL}}{\sin \alpha} [\cos \theta - \Gamma \sin \theta], \end{aligned} \tag{4.7}$$

where

$$\Gamma = \frac{\gamma + \cos(\theta - \alpha)}{\sin(\theta - \alpha)}. \tag{4.8}$$

The quantity $-\frac{\partial \Delta G}{\partial \tau}$ is related to the cooling rate and is denoted as C . As crystallisation proceeds to completion, $\theta \rightarrow \frac{1}{2}\pi$, and the final value of C is

$$C = 2\Gamma \left[\sigma_{AL} + \frac{\sigma_{PL}}{\sin \alpha} \right] - \frac{\gamma\sigma_{PP}}{\sin \alpha} - 2\sigma_{AP}(1 + \Gamma^2)^{1/2}, \tag{4.9}$$

and

$$\Gamma = \frac{\gamma + \sin \alpha}{\cos \alpha}; \tag{4.10}$$

as before, the final dihedral angle is

$$\Delta = 2 \tan^{-1} \Gamma, \tag{4.11}$$

while the impingement angle is $\psi = 2\alpha$.

We require that $C \geq 0$ in (4.9). In fact, we might argue that in practice this should be prescribed, and that this determines the relative growth rate γ . The sign of C clearly depends on the interfacial energies. Not much is known about these. One constraint is the augite-plagioclase equilibrium dihedral angle. Although anisotropy of grain boundary energies means that there is a range of equilibrium angles, depending on the relative orientation of the three grains involved, if we

assume a single value of 109° (i.e. the median of the population of equilibrium angles), this implies that

$$\sigma_{PP} = 1.16 \sigma_{AP}. \tag{4.12}$$

Another lies in the fact that the liquid does not wet the A–P grain boundary, which implies that

$$\sigma_{AP} < \sigma_{AL} + \sigma_{PL}, \tag{4.13}$$

as also used in Sect. 3.

We note from Fig. 5 of part 1 that for $\psi \gtrsim \Theta_{cpp}^*$, the increasing trend of the dihedral angle Δ is flattened. We note also that if $\gamma > 0$, then (4.10) implies $\Gamma > \tan \alpha$ and thus $\Delta > \psi$, whereas if $\gamma < 0$ (plagioclase re-melting), $\Delta < \psi$. This suggests that the flattening at $\psi \approx \Theta_{cpp}^*$ is associated with passage of γ through zero and the localised dissolution of plagioclase. Why should this occur? If we use (4.9) to compute the final value of C if $\gamma = 0$, we find

$$C = C_0 = 2 \sec \alpha [\sigma_{AL} \sin \alpha + \sigma_{PL} - \sigma_{AP}]. \tag{4.14}$$

Suppose for illustration, and in keeping with (4.13), that we can define an angle ω via

$$\sigma_{AP} = \sigma_{AL} \sin \omega + \sigma_{PL}, \tag{4.15}$$

then

$$C_0 = 2\sigma_{AL} \sec \alpha [\sin \alpha - \sin \omega], \tag{4.16}$$

which shows that passage of γ through zero can be associated with C also reaching zero at the particular impingement angle $\psi = 2\omega$. This suggests that we associate the flattening of the curve in Fig. 5 of part 1 with plagioclase dissolution.

In order to examine this, we need to provide a recipe for cooling which maintains a positive value for C all the way to final crystallisation. A simple such recipe is to prescribe a constant final value of C . That is, we use (4.9) and (4.10) to determine γ and Γ (and thus Δ) for given $\psi = 2\alpha$. Figure 11 shows the result of this for various values of C . Note that the units of ΔG are $J m^{-1}$, and thus those of C are $J m^{-2}$, since τ has units of m . To be specific, we define the dimensionless quantity

$$C^* = \frac{C}{\sigma_{AP}} = 2\Gamma \left[s_{AL} + \frac{s_{PL}}{\sin \alpha} \right] - \frac{\gamma s_{PP}}{\sin \alpha} - 2(1 + \Gamma^2)^{1/2}, \tag{4.17}$$

where

$$s_{AL} = \frac{\sigma_{AL}}{\sigma_{AP}}, \quad s_{PL} = \frac{\sigma_{PL}}{\sigma_{AP}}, \quad s_{PP} = \frac{\sigma_{PP}}{\sigma_{AP}}, \tag{4.18}$$

and plot in Fig. 11 the resulting curves for $\Delta(\psi)$ for various values of C^* .

It is clear, at least with these parameter values, that the dihedral angle eventually flattens as is suggested by Fig. 5 of part 1. Of course, the shapes of the curves depend on the

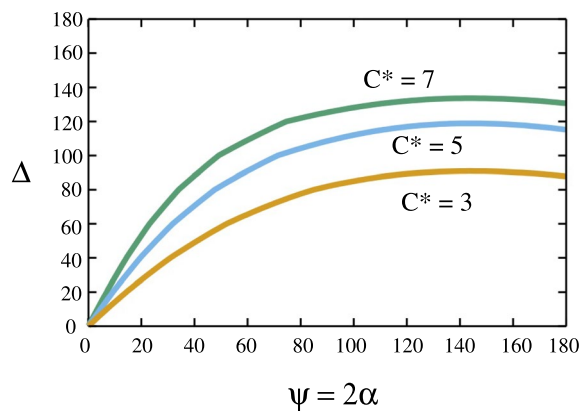


Fig. 11 The final dihedral angle Δ as a function of impingement angle ψ , for values of $C^* = 3, 5, 7$, and with $s_{PP} = 1.16$, $s_{AL} = 0.5$, and $s_{PL} = 1.88$

choices for the interfacial energies. It is perhaps of interest that the choice used in Fig. 11 was the initial choice. The value of s_{AL} is based on an egalitarian view of (4.13). The larger value of s_{PL} , however, is based on the following consideration. Although there are no impingement angles greater than 144° in Fig. 5 of part 1, one might argue that this is due to a sparsity of sampling. High impingement angles are likely to lead to impingement with other crystals which renders the high impingement angles invisible. On the other hand, we might suppose that 144° represents an upper bound for the impingement angle. Based on the fact that surface energy diminution requirements at plagioclase-plagioclase-liquid junctions with impingement angle ψ require

$$\cos \frac{1}{2}\psi > \frac{\sigma_{PP}}{2\sigma_{PL}}, \tag{4.19}$$

the maximum observed angle of $\approx 144^\circ$ might suggest that

$$\sigma_{PP} = 2\sigma_{PL} \cos 72^\circ = 0.618 \sigma_{PL}, \tag{4.20}$$

it is this choice which motivated the value $s_{PL} = 1.88 = 1.16/0.618$ in the figure.³

Our theory of localised plagioclase dissolution appears to account for the data in Fig. 5 of part 1 and is consistent with a close inspection of high impingement/dihedral angle junctions, where the final angle appears to be caused by a late alteration of the dihedral interface. This is indicated in Fig. 2. Of course the reverse curvature of eagles’ beaks also contributes to this effect, and one can also interpret some of the sketches in Fig. 2 in this way.

³ The number 0.618 is the golden ratio (or its inverse), and is due to the fact that $\cos 72^\circ = \frac{1}{4}(\sqrt{5} - 1)$, a surprising but easily verified fact.

Of possible concern is that the curves in Fig. 11 all have $\Delta \rightarrow 0$ as $\psi \rightarrow 0$; and specifically

$$\Delta \sim \frac{[C^* - s_{PP} + 2]\psi}{2s_{PL} - s_{PP}}. \quad (4.21)$$

While this is not inconsistent with Fig. 5 of part 1, we consider it more likely that Fig. 6 applies with $0 < \gamma < 1$, since the importance of the surface energy reduction rate in (4.9) is presumably only of significance if C approaches zero.

Discussion and conclusions

We argue that a simple geometric theory of crystal growth has the potential to explain the two principal observations we provided in the companion paper: firstly, the classification of APP three-grain junctions into three types, of which the third, eagles' beaks, is perhaps the most puzzling; and secondly, the variation of dihedral angle with impingement angle, with the particular flattening at high impingement angle. While our explanation for grain boundary configuration types 1 and 2, and our explanation of the dihedral angle spread at impingement angle $\lesssim 100^\circ$ is straightforward, our explanation of the eagles' beaks, and the dihedral angle flattening at large impingement angle, both rely on more subtle descriptions of the growth of plagioclase grains.

Type 1 and 2 morphologies can be understood as a simple geometrical consequence of interfacial growth following augite-plagioclase impingement. Type 3 can be explained by consideration of what occurs when an impinged augite crystal reaches the corner of a plagioclase grain. In our description, the polar angle θ from the centre of the augite grain increases as the A–P–melt junction progresses (upwards) along the long plagioclase face; however, after it turns the corner and marches along the short face, θ must decrease. Eagles' beaks are associated with the idea that this jump in the rate of change of θ can not occur instantly, but rather is mediated by a transient period while the augite interface is locked to the corner of the plagioclase grain while the curvature-controlled interfacial angle adjusts to its new circumstance. As indicated in Fig. 8, this causes the curvature of the evolving grain boundary to reverse, thus forming the eagle's beak. This conjecture can be formulated as a problem in interfacial growth, much of which is described in the electronic supplementary material, but its detailed solution is beyond the remit of the present paper, and awaits development in a future, more technically complex, theoretical exposition.

Our explanation associates eagles' beaks with crystal mushes in which augite grains can reach the ends of the tabular faces. This requires that the plagioclase grains grow simultaneously with the augite grains, and in particular that the plagioclase has not formed a scaffold into which

the augite can grow. This is exactly the conclusion which was drawn in part 1 from observation, that eagles' beaks were preponderant in gabbros and highly orthocumulate troctolites.

In appealing to interfacial energy equilibrium at an A–P–melt corner, we follow Jackson and Hunt's (1966) theory of lamellar eutectic growth. In fact this constraint should *always* apply at such a corner, which suggests that the interfacial growth rate of grains is necessarily modified once impingement has occurred.

This latter idea underlies our further explanation of the dihedral angle flattening which was seen in Fig. 5 of part 1. As pores close off, the interfacial energy considerations at a corner extend to a critical constraint on the rates of grain boundary growth, and it seems that in this case, plagioclase dissolution may occur, with the consequent flattening seen in Fig. 11.

Figure 2 showed illustrations of various high dihedral angle junctions. They can of course be interpreted in different ways. The parallel lines indicate the tabular faces of the plagioclase. Sketches (a), (b) and (c) are consistent with our description of eagles' beaks, with the red lines indicating the reversed curvature following augite reaching the plagioclase corner. Sketch (d) is rather different, as the red line of reversed curvature suggests growth towards an eagle's beak, but the blue line suggests that the augite stops growing during the last stages of junction formation. We suppose this is due to the interfacial energy constraints discussed earlier.

It should be emphasised that the theory provided here is somewhat simplified, but we think that we have demonstrated that the energy of melt/solid interfaces becomes an important constraining factor on crystallisation in mushes once impingement has occurred (and thus roughly when they become immobile).

Disequilibrium dihedral angles have the potential to provide a powerful probe of the thermal history of fully solidified dolerites and gabbros. Of particular interest is the variation of cooling rate as a function of fractionation in layered intrusions. The analysis in the present contribution represents the first step towards the full quantification of dihedral angle formation that is a requirement for the interpretation of Θ_{cpp} variation and its use as a proxy for the fractional contribution of latent heat to the enthalpy budget of layered intrusions.

Supplementary Information The online version contains supplementary material available at <https://doi.org/10.1007/s00410-022-01921-w>.

Acknowledgements A. C. F. acknowledges the support of the Mathematics Applications Consortium for Science and Industry (<http://www.macs.ul.ie>) funded by the Science Foundation Ireland mathematics grant 12/IA/1683. M. B. H. acknowledges the support of the the Natural Environment Research Council (Grant number NE/N009894/1). The authors would like to thank the Isaac Newton Institute for Mathematical Sciences, Cambridge, for support and hospitality during the

programme ‘Melt in the mantle’ where work on this paper was undertaken. This work was supported by EPSRC Grant no EP/K032208/1.

Open Access This article is licensed under a Creative Commons Attribution 4.0 International License, which permits use, sharing, adaptation, distribution and reproduction in any medium or format, as long as you give appropriate credit to the original author(s) and the source, provide a link to the Creative Commons licence, and indicate if changes were made. The images or other third party material in this article are included in the article's Creative Commons licence, unless indicated otherwise in a credit line to the material. If material is not included in the article's Creative Commons licence and your intended use is not permitted by statutory regulation or exceeds the permitted use, you will need to obtain permission directly from the copyright holder. To view a copy of this licence, visit <http://creativecommons.org/licenses/by/4.0/>.

References

- Davis SH (2001) Theory of solidification. C.U.P, Cambridge
- Dowty E (1980) Crystal growth and nucleation theory and the numerical simulation of igneous crystallisation. In: Hargraves RB (ed) Physics of magmatic processes. Princeton University Press, Princeton, pp 419–485
- Flemings MC (1974) Solidification processing. McGraw-Hill, New York
- Holness MB (2014) The effect of crystallization time on plagioclase grain shape in dolerites. *Contrib Mineral Pet* 168(1):076
- Holness MB (2015) Plagioclase growth rates control three-grain junction geometry in dolerites and gabbros. *J Petrol* 56:2117–2144
- Holness MB, Humphreys MCS, Sides R, Helz RT, Tegner C (2012) Towards an understanding of disequilibrium dihedral angles in mafic rocks. *J Geophys Res* 117(B6):B06207
- Jackson KA, Hunt JD (1966) Lamellar and rod eutectic growth. *Trans Metall Soc AIME* 236(8):1129–1141
- Kath WL, Cohen DS (1982) Waiting-time behavior in a nonlinear diffusion equation. *Stud Appl Math* 67:79–105
- Kelton KF, Greer AL (2010) Nucleation in condensed matter: applications in materials and biology. Elsevier (Pergamon Materials Series), Amsterdam
- Lacey AA, Ockendon JR, Tayler AB (1982) “Waiting-time” solutions of a nonlinear diffusion equation. *SIAM J Appl Math* 42(6):1252–1264

Publisher's Note Springer Nature remains neutral with regard to jurisdictional claims in published maps and institutional affiliations.